JACS
JOURNAL OF THE AMERICAN CHEMICAL SOCIETY
Article
pubs.acs.org/JACS

Multifunctional Phosphate-Based Inorganic–Organic Hybrid Nanoparticles

Joachim G. Heck,[†] Joanna Napp,[‡] Sara Simonato,[†] Jens Möllmer,[§] Marcus Lange,[§] Holger M. Reichardt,[∥] Reiner Staudt,[§,⊥] Frauke Alves,*[,‡] and Claus Feldmann*[,†]

[†]Institute of Inorganic Chemistry, Karlsruhe Institute of Technology (KIT), Engesserstraße 15, 76131 Karlsruhe, Germany

[‡]Max-Planck-Institute for Experimental Medicine, Dept. Molecular Biology of Neuronal Signals, Hermann-Rein-Straße 3, 37075 Göttingen, Germany

[§]Institut für Nichtklassische Chemie e.V., Permoserstraße 15, 04318 Leipzig, Germany

[∥]University of Göttingen Medical School, Institute for Cellular and Molecular Immunology, Humboldtallee 34, 37073 Göttingen, Germany

[⊥]University of Applied Sciences Offenburg, Badstraße 24, 77652 Offenburg, Germany

Supporting Information

ABSTRACT: Phosphate-based inorganic–organic hybrid nanoparticles (IOH-NPs) with the general composition $[M]^{2+}[R_{function}(O)PO_3]^{2-}$ (M = ZrO, Mg_2O; R = functional organic group) show multipurpose and multifunctional properties. If $[R_{function}(O)PO_3]^{2-}$ is a fluorescent dye anion ($[R_{dye}OPO_3]^{2-}$), the IOH-NPs show blue, green, red, and near-infrared fluorescence. This is shown for $[ZrO]^{2+}[PUP]^{2-}$, $[ZrO]^{2+}[MFP]^{2-}$, $[ZrO]^{2+}[RRP]^{2-}$, and $[ZrO]^{2+}[DUT]^{2-}$ (PUP = phenylumbelliferon phosphate, MFP = methylfluorescein phosphate, RRP = resorufin phosphate, DUT = Dyomics-647 uridine triphosphate). With pharmaceutical agents as functional anions ($[R_{drug}OPO_3]^{2-}$), drug transport and release of anti-inflammatory ($[ZrO]^{2+}[BMP]^{2-}$) and antitumor agents ($[ZrO]^{2+}[FdUMP]^{2-}$) with an up to 80% load of active drug is possible (BMP = betamethason phosphate, FdUMP = 5′-fluoro-2′-deoxyuridine 5′-monophosphate). A combination of fluorescent dye and drug anions is possible as well and shown for $[ZrO]^{2+}[BMP]^{2-}{}_{0.996}[DUT]^{2-}{}_{0.004}$. Merging of functional anions, in general, results in $[ZrO]^{2+}([R_{drug}OPO_3]_{1-x}[R_{dye}OPO_3]_x)^{2-}$ nanoparticles and is highly relevant for theranostics. Amine-based functional anions in $[MgO]^{2+}[R_{amine}PO_3]^{2-}$ IOH-NPs, finally, show CO_2 sorption (up to 180 mg g^{-1}) and can be used for CO_2/N_2 separation (selectivity up to α = 23). This includes aminomethyl phosphonate $[AMP]^{2-}$, 1-aminoethyl phosphonate $[1AEP]^{2-}$, 2-aminoethyl phosphonate $[2AEP]^{2-}$, aminopropyl phosphonate $[APP]^{2-}$, and aminobutyl phosphonate $[ABP]^{2-}$. All $[M]^{2+}[R_{function}(O)PO_3]^{2-}$ IOH-NPs are prepared via noncomplex synthesis in water, which facilitates practical handling and which is optimal for biomedical application. In sum, all IOH-NPs have very similar chemical compositions but can address a variety of different functions, including fluorescence, drug delivery, and CO_2 sorption.

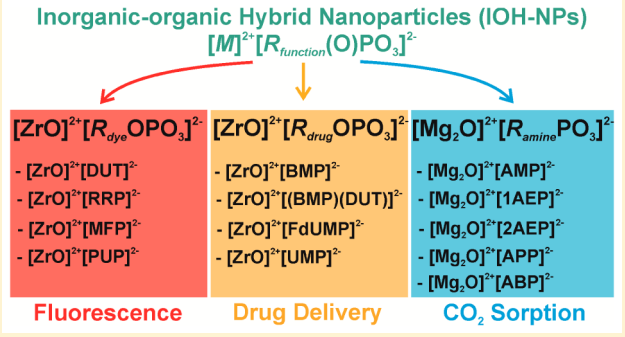

1. INTRODUCTION

Hybrid nanomaterials are intensely discussed for various purposes—including catalysis,[1] theranostics,[2] sensors,[3] solar cells,[4] and gas sorption[5] as well as magnetic,[6] plasmonic,[7] or optoelectronic properties[8]—and allow for unique merging of different constituents to realize optimally adapted multipurpose and/or multifunctional properties. Most often specific nanoparticles or molecules have been incorporated into polymers.[9] Furthermore, carbon species such as carbon nanotubes (CNTs), graphene, carbon dots (C-dots), or Fullerenes have been integrated into oxides (e.g., SiO_2) or polymers.[10] Nanostructured hybrid biomaterials have been widely discussed as well in view of biocompatibility and biodegradability, for instance, in regenerative medicine, for biorecognition, or as biosensors and biopolymers.[11]

The concept of inorganic–organic hybrids emerged about 30 years ago with the expansion of soft inorganic chemistry processes.[12] Ever since, mild synthesis conditions have allowed a flexible mixing of inorganic and organic constituents on the nanoscale and, thereby, the realization of tailor-made materials with specific chemical and physical properties.[1−11] However, it must be noted that many hybrid materials are not nanoparticles on the whole, but contain nanoscaled constituents (e.g., nanoparticles, nanorods, nanolayers) embedded in a macro-

Received: February 3, 2015
Published: May 27, 2015

DOI: 10.1021/jacs.5b01172
J. Am. Chem. Soc. 2015, 137, 7329−7336

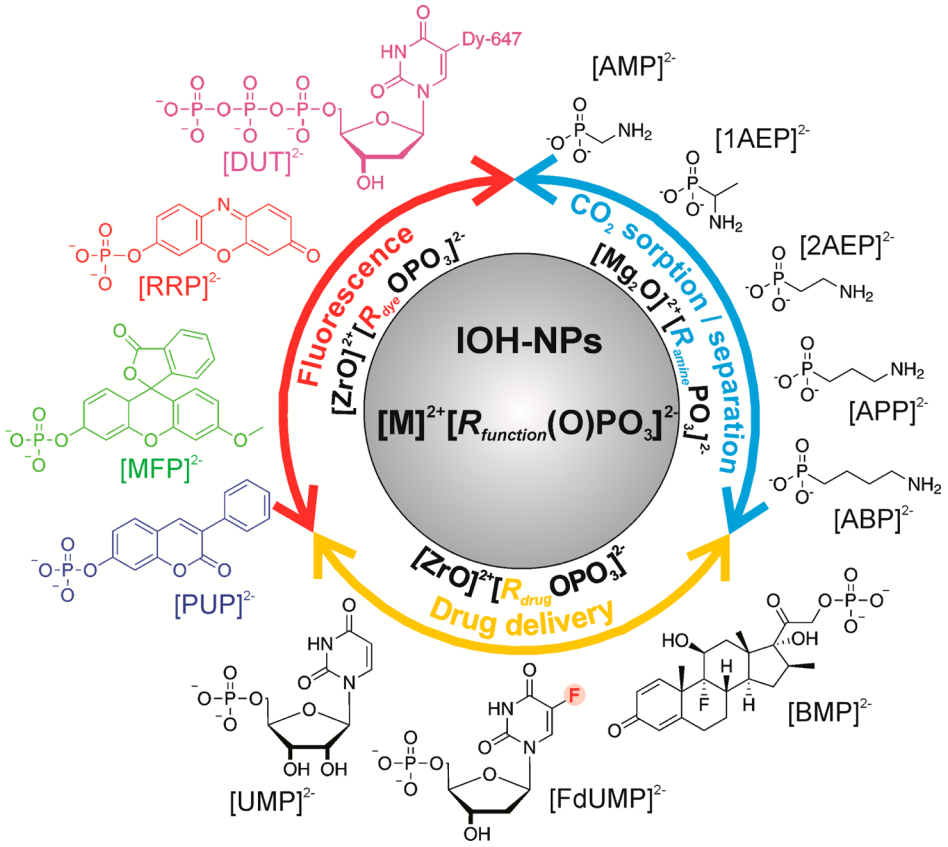

Figure 1. Scheme illustrating the composition and the multipurpose properties of the inorganic–organic hybrid nanoparticles (IOH-NPs) $[M]^{2+}[R_{function}(O)PO_3]^{2-}$ (M = ZrO, Mg_2O; R = functional organic group). The IOH-NPs are composed of equimolar amounts of an inorganic cation ($[ZrO]^{2+}$, $[Mg_2O]^{2+}$) and a functional organic anion ($[R_{dye}OPO_3]^{2-}$, $[R_{drug}OPO_3]^{2-}$, $[R_{amine}PO_3]^{2-}$) with a phosphate or phosphonate group. Exceptional loads of up to 80 wt % of fluorescent organic dyes and pharmaceutical agents are possible.

scopic matrix. But real hybrid nanomaterials are as well available today with complex compositions and fascinating structures addressing multimodal functions with high adaptability.[13] On the other hand, the complexity and sheer number of constituents can be a limitation by itself. Apart from advanced synthesis and demanding handling, for instance, *in vivo* biomedical application can be restricted since all constituents and all types of combinations might need individual clinical approval.

In the following, we present phosphate-based inorganic–organic hybrid nanoparticles (IOH-NPs) as a new material concept. Similar to simple sodium chloride, containing equimolar amounts of Na^+ cations and Cl^- anions, the IOH-NPs consist of equimolar amounts of an inorganic cation—$[ZrO]^{2+}$ or $[Mg_2O]^{2+}$—and a functional organic anion $[R_{function}(O)PO_3]^{2-}$ (R: organic group) containing a phosphate or phosphonate group. Whereas the organic anion entails a specific function such as fluorescence (with $[R_{dye}OPO_3]^{2-}$), drug release (with $[R_{drug}OPO_3]^{2-}$), or CO_2 sorption (with $[R_{amine}PO_3]^{2-}$), the predominant role of the inorganic cation is to make the hybrid nanomaterial an insoluble compound. Insolubility (in water) is essential to allow for controlled nucleation and growth of nanoparticles via aqueous precipitation. Based on noncomplex water-based synthesis, adaptable composition, a flexible combination of properties (including fluorescence, drug delivery, CO_2 sorption, CO_2 separation), an enormous dye/drug load (up to 80 wt %), the IOH-NPs can be a promising alternative to existing nanoscale functional materials.

2. EXPERIMENTAL SECTION

Synthesis of Phosphate-Based IOH-NPs $[M]^{2+}[R_{function}(O)PO_3]^{2-}$. $[ZrO]^{2+}[R_{dye}OPO_3]^{2-}$ and $[ZrO]^{2+}[R_{drug}OPO_3]^{2-}$ IOH-NPs are prepared by noncomplex admixing of aqueous solutions of $ZrOCl_2 \cdot 8H_2O$ and either the acid form or the sodium salt of the relevant functional organic anion. Moreover, the parameters to control particle nucleation and growth must be considered (including speed of mixing, temperature, duration or reaction; for details, see: Supporting Information (SI): Synthesis). $[Mg_2O]^{2+}[R_{amine}PO_3]^{2-}$ IOH-NPs can be prepared similarly. Aiming at low molar weight, however, zirconium was exchanged by magnesium. In view of the small particle size and specific surface area, moreover, we have performed the synthesis in the volume-restricted water pool of a water-in-oil microemulsion (SI: Synthesis). All nanoparticles were washed and separated as powder samples. For biomedical application, the as-prepared nanoparticles were redispersed into HEPES-buffer (30 mM) or dextran 40 (1.6 mg mL^{-1}).

3. RESULTS AND DISCUSSION

3.1. Synthesis of $[M]^{2+}[R_{function}(O)PO_3]^{2-}$ IOH-NPs. The here presented IOH-NPs can include a wide range of different compounds with the general composition $[M]^{2+}[R_{function}(O)PO_3]^{2-}$ (M = ZrO, Mg_2O; R = functional organic group). This variety is possible since functional organic anions containing a phosphate or phosphonate group typically turn into insoluble salts upon addition of $[ZrO]^{2+}$ or $[Mg]^{2+}$ as a cation (Figure 1). As a result, we can show 13 different types of nanoparticles: $[ZrO]^{2+}[PUP]^{2-}$, $[ZrO]^{2+}[MFP]^{2-}$, $[ZrO]^{2+}[RRP]^{2-}$, $[ZrO]^{2+}$-$[DUT]^{2-}$, $[ZrO]^{2+}[BMP]^{2-}$, $[ZrO]^{2+}[FdUMP]^{2-}$, $[ZrO]^{2+}$-$[UMP]^{2-}$, $[ZrO]^{2+}[BMP]^{2-}{}_{0.996}[DUT]^{2-}{}_{0.004}$, $[MgO]^{2+}$-

DOI: 10.1021/jacs.5b01172
J. Am. Chem. Soc. 2015, 137, 7329–7336

$[AMP]^{2-}$, $[MgO]^{2+}[1AEP]^{2-}$, $[MgO]^{2+}[2AEP]^{2-}$, $[MgO]^{2+}$-$[APP]^{2-}$, and $[MgO]^{2+}[ABP]^{2-}$ (PUP = phenylumbelliferon phosphate, MFP = methylfluorescein phosphate, RRP = resorufin phosphate, DUT = Dyomics-647 uridine triphosphate, BMP = betamethason phosphate, FdUMP = 5′-fluoro-2′-deoxyuridine 5′-monophosphate, UMP = uridine monophosphate, AMP = aminomethyl phosphonate, 1AEP = 1-aminoethyl phosphonate, 2AEP = 2-aminoethyl phosphonate, APP = aminopropyl phosphonate, ABP = aminobutyl phosphonate $[ABP]^{2-}$) (Figure 1).

As all IOH-NPs are insoluble in water, they can be prepared via straightforward precipitation in water (Figure 2a; SI: Synthesis).[14] To obtain nanoparticles and colloidally stable aqueous suspensions, LaMer's well-known concept for controlling particle nucleation and growth must be considered.[15] According to scanning electron microscopy (SEM) and dynamic light scattering (DLS), the as-prepared IOH-NPs exhibit typical mean diameters of 20−40 nm (Figure 2c; statistical evaluation of SEM images given in the SI: Table S1, Figure S1) and hydrodynamic diameters in the 40−90 nm range (Figure 2b; SI: Figure S2). Aqueous suspensions with typical IOH-NP concentrations of 1−10 wt % are colloidally stable for weeks.

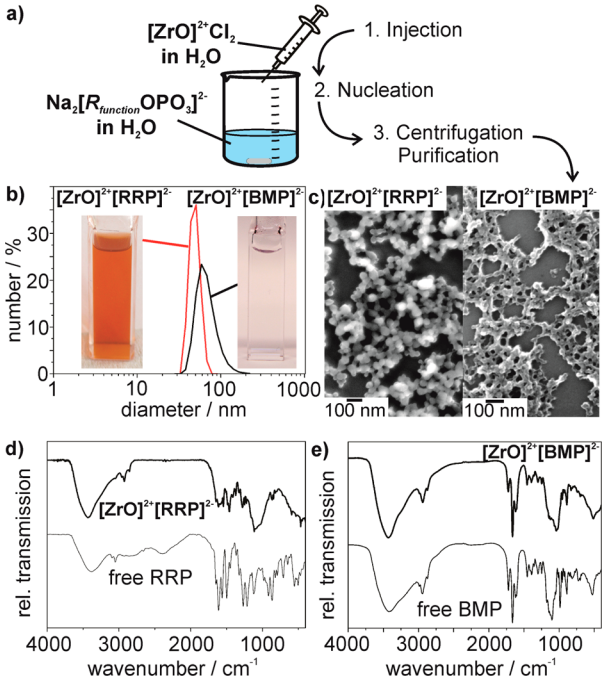

Figure 2. Water-based synthesis of IOH-NPs results in colloidally stable aqueous suspensions as exemplarily shown for $[ZrO]^{2+}[RRP]^{2-}$ and $[ZrO]^{2+}[BMP]^{2-}$: (a) Scheme illustrating the water-based synthesis; (b) Size and size distribution according to DLS (with photos of suspensions; (c) Size and size distribution according to SEM; (d,e) FT-IR spectra of $[ZrO]^{2+}[RRP]^{2-}$ and $[ZrO]^{2+}[BMP]^{2-}$ with the starting materials $H_2[RRP]$ and $Na_2[BMP]$ as references.

In view of the chemical composition of the IOH-NPs, the presence of the functional organic anion and the inorganic cation is most important. This is evidenced via infrared spectroscopy (FT-IR) and energy-dispersive X-ray analysis (EDX) (Figure 2d,e; SI: Figures S3−S8). Furthermore, it should be noted that the presence of both the cation and anion is essential for obtaining an insoluble compound. The cation-to-anion ratio of 1:1 (Zr:P) and 2:1 (Mg:P) is verified by different analytical techniques, including EDX, inductively coupled plasma atomic emission spectroscopy (ICP-AES), thermogravimetry (TG), and elemental analysis (EA) (SI: Table S2). As a result, the compositions $[ZrO]^{2+}[R_{dye}OPO_3]^{2-}$, $[ZrO]^{2+}[R_{drug}OPO_3]^{2-}$, and $[Mg_2O]^{2+}[R_{amine}PO_3]^{2-}$ are verified for the IOH-NPs (SI: Table S2). It is remarkable that all IOH-NPs are noncrystalline.

3.2. Full Color Emission of $[ZrO]^{2+}[R_{dye}OPO_3]^{2-}$ IOH-NPs. In general, fluorescent nanoparticles are promising tools for applications in medicine and molecular biology.[16] Together with optical imaging techniques, they allow for *in vivo* as well as *ex vivo* diagnostic strategies and monitoring of complex biological processes. In this regard, semiconductor-type quantum dots (e.g., CdSe)[17] and rare-earth-doped oxides/fluorides (e.g., $LaPO_4$:Eu, $NaYF_4$:Er,Yb)[18] are well established. Moreover, composite nanoparticles with surface-attached fluorescent dyes or fluorescent dyes encapsulated into certain oxide matrices (e.g., SiO_2, $Ca_3(PO_4)_2$) have been described.[19] In view of this, fluorescent IOH-NPs comprise meaningful advantages: (*i*) Harmful elements such as Cd, Hg, Pb, Se, or Te are excluded; (*ii*) as the fluorescence of the IOH-NPs originates from the dye anion, special efforts related to precise size control (for achieving quantum-size effects), high crystallinity, and core−shell structures (for avoiding defect-related relaxation) are obsolete; (*iii*) nanoparticle synthesis in water is optimal for application in medicine. All these aspects facilitate materials synthesis considerably.

Full color emission of $[ZrO]^{2+}[R_{dye}OPO_3]^{2-}$ IOH-NPs is shown with phenylumbelliferon phosphate ($[PUP]^{2-}$), methylfluorescein phosphate ($[MFP]^{2-}$), resorufin phosphate ($[RRP]^{2-}$), and Dyomics-647 uridine triphosphate ($[DUT]^{2-}$) as organic dye anions, showing blue (380−600 nm, λ_{max} = 458 nm), green (460−700 nm, λ_{max} = 518 nm), red (550−700 nm, λ_{max} = 584 nm), and near-infrared (630−780 nm, λ_{max} = 675 nm) emission, respectively (Figure 3a,b; SI: Figure S9). Due to the quasi-infinite number of fluorescence centers, the IOH-NPs show intense spot-light emission in aqueous suspension (Figure 3b). Even partial bleaching of the fluorescent dye is less of a limitation due to the molar dye reservoir (dye content up to 80 wt %, SI: Table S1) in each single IOH-NP.

Biomedical issues and optical imaging-based applications in animal models and in humans require long-wavelength emission rather than in the far-red and near-infrared range, as the light absorption by water and hemoglobin is minimal in this spectral range, resulting in optimal tissue penetration.[16,20] In this respect, $[ZrO]^{2+}[MFP]^{2-}$, $[ZrO]^{2+}[RRP]^{2-}$, and $[ZrO]^{2+}[BMP]^{2-}{}_{0.996}[DUT]^{2-}{}_{0.004}$ were incubated *in vitro* with cultured murine alveolar macrophages of the MH-S cell line[21] (50 μg mL^{-1} of cell culture medium) to analyze the uptake as well as the potential of IOH-NPs for imaging applications. After 5 h of incubation at 37 °C, a clear internalization of all IOH-NPs by macrophages was demonstrated by fluorescence microscopy (data not shown), which was even more evident after 24 h (Figure 3c). The granularly structured fluorescence in the cells (in contrast to the cell nuclei) indicates the presence of nanoparticles (Figure 3c) that was also confirmed by electron-energy loss spectroscopy showing a similar granular structure for the localization of zirconium in the macrophages (SI: Figure S11).[14b] In both control assays—including (*i*) MH-S cells incubated with the nanoparticles at 4 °C where the cellular metabolism and therefore internalization is strongly reduced and (*ii*) MH-S cells

DOI: 10.1021/jacs.5b01172
J. Am. Chem. Soc. 2015, 137, 7329−7336

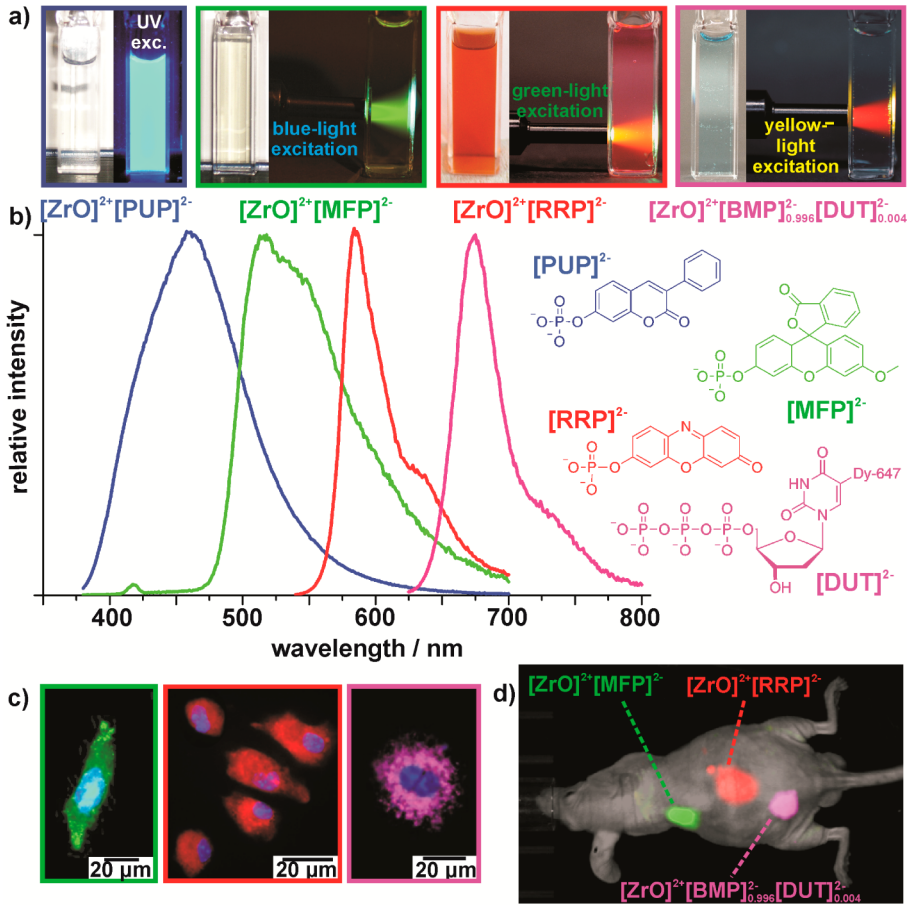

Figure 3. Fluorescence of $[ZrO]^{2+}[R_{dye}OPO_3]^{2-}$ IOH-NPs: (a) Nanoparticles in aqueous suspensions (excitation via halogen lamp with light fiber and color filter for obtaining blue, green, or yellow light; blue-emitting $[ZrO]^{2+}[PUP]^{2-}$ excited with UV-lamp); (b) Emission spectra and chemical composition of $[ZrO]^{2+}[PUP]^{2-}$ (blue), $[ZrO]^{2+}[MFP]^{2-}$ (green), $[ZrO]^{2+}[RRP]^{2-}$ (red), $[ZrO]^{2+}[BMP]^{2-}{}_{0.996}[DUT]^{2-}{}_{0.004}$ (magenta; combined with anti-inflammatory drug $[BMP]^{2-}$); (c) Fluorescence microscopy showing the uptake of $[ZrO]^{2+}[MFP]^{2-}$ (green), $[ZrO]^{2+}[RRP]^{2-}$ (red), or $[ZrO]^{2+}[BMP]^{2-}{}_{0.996}[DUT]^{2-}{}_{0.004}$ (magenta; combined with anti-inflammatory drug $[BMP]^{2-}$) by MHS macrophages (cell nuclei show blue emission due to 4′,6-diamidin-2-phenylindole (DAPI) staining), (d) Spectrally unmixed fluorescence intensity map of a nude mouse after subcutaneous injection of $[ZrO]^{2+}[MFP]^{2-}$, $[ZrO]^{2+}[RRP]^{2-}$, and $[ZrO]^{2+}[BMP]^{2-}{}_{0.996}[DUT]^{2-}{}_{0.004}$ (each in a concentration of 10 μg in 50 μL of 0.9% NaCl).

cultivated without nanoparticles—no comparable fluorescence was observed within the cells (data not shown). Furthermore, no toxic effects of phosphate-based $[ZrO]^{2+}[R_{function}OPO_3]^{2-}$ IOH-NPs could be determined with concentrations up to 250 μM (SI: Figure S12), showing their biocompatibility.

The capability of the IOH-NPs for *in vivo* optical imaging was confirmed by proof-of-concept experiments. Here, fluorescence signals derived from subcutaneously injected $[ZrO]^{2+}[MFP]^{2-}$, $[ZrO]^{2+}[RRP]^{2-}$, and $[ZrO]^{2+}[BMP]^{2-}{}_{0.996}[DUT]^{2-}{}_{0.004}$ (10 μg of each) were measured in a living mouse using an IVIS spectrum *in vivo* imager. Application of a spectral unmixing protocol allowed clear identification and separation of fluorescence signals derived from each particular IOH-NP type (Figure 3d).

3.3. Drug Delivery of $[ZrO]^{2+}[R_{drug}OPO_3]^{2-}$ IOH-NPs. Despite tremendous advances in clinical diagnostic techniques and therapeutic strategies, there is still a high demand for engineering new tools for both diagnostic and therapeutic purposes, especially, in terms of increased sensitivity and reduced treatment side effects. Nanoparticle-based technologies that emerged in the recent decades, although innovative, are still far from being perfect. Especially, nonbiocompatible materials that need to be encapsulated or covered with well-tolerable agents, with unknown or uncertain systemic clearance of the body, are still a major drawback toward the translation of nanotechnology into clinical practice. Recently, a branch of molecular technologies that incorporate both diagnostic and therapeutic functionalities, so-called theranostics, have attracted enormous interest to improve patient management via personalization of therapeutic interventions.[2,19] Here, nanoformulations offer perfect tools, as they can easily include a defined combination of agents and functions within a single particle. Therefore, new nanoformulations with a high load of active agents that are less harmful and preferentially based on already existing or even clinically approved materials are in high demand for clinical application.

Similar to the widely applied nucleoside phosphate prodrugs,[22] the P−O−C bond in the functional anions $[R_{drug}OPO_3]^{2-}$ is slowly hydrolyzed in physiological media by phosphatases, which induces the release of the active agent from the phosphate-based IOH-NPs (Figure 4a, SI: Figure S10). Thus, the IOH-NPs dissolve into the drug molecule and zirconyl phosphate. Phosphate is excreted via normal metabolic activity, and zirconium (as $[ZrO]^{2+}$) is of low toxicity and known to be well-tolerable to the human body (>1 g kg^{-1}).[23] Such dissolution is favored for theranostics, especially for *in vivo*

DOI: 10.1021/jacs.5b01172
J. Am. Chem. Soc. 2015, 137, 7329−7336

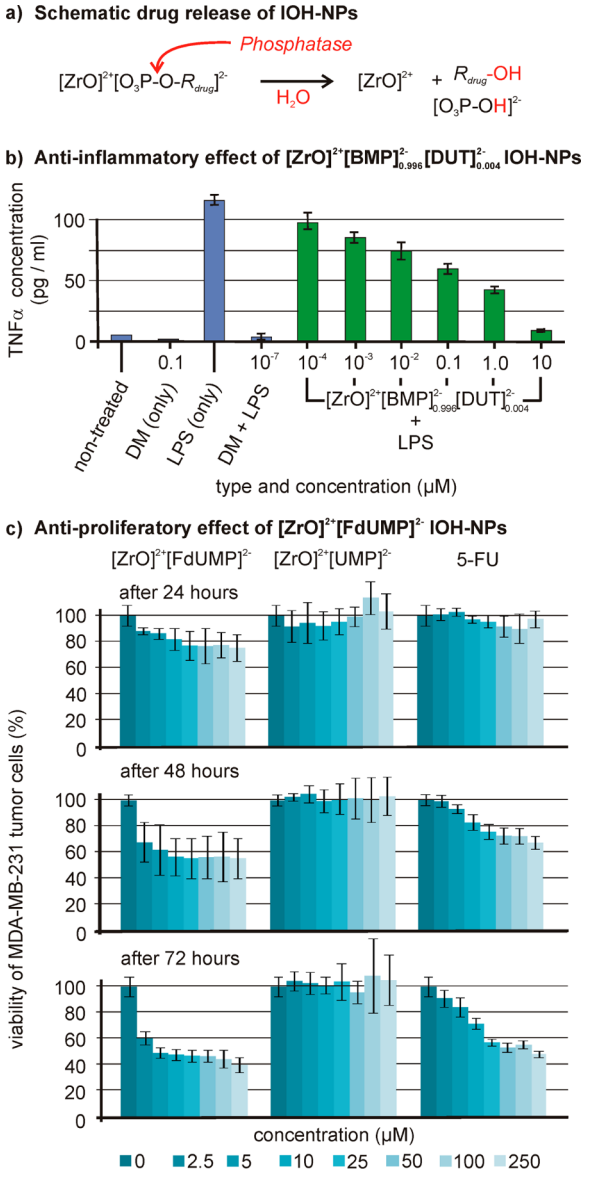

Figure 4. Drug release of $[ZrO]^{2+}[R_{drug}OPO_3]^{2-}$ with betamethasone phosphate ($[BMP]^{2-}$) and 5-fluoruridine phosphate ($[FdUMP]^{2-}$) as examples: (a) Scheme illustrating the phosphatase-mediated release under physiological conditions;[22] (b) TNFα concentration in the cell culture supernatant as a measure of the anti-inflammatory activity of $[ZrO]^{2+}[BMP]^{2-}_{0.996}[DUT]^{2-}_{0.004}$ in comparison to untreated, DM-treated, LPS-treated, and LPS+DM-treated MH-S macrophages; (c) Antiproliferatory activity of $[ZrO]^{2+}[FdUMP]^{2-}$ on MDA-MB-231 mamma carcinoma cells as compared to nonactive $[ZrO]^{2+}[UMP]^{2-}$ (UMP: uridine monophosphate) as negative control, and the molecular drug 5-FU (5-FU: 5-fluoruracil) as positive control.

application in humans.[24] Both drug release and treatment efficacy of IOH-NPs were investigated in proof-of-concept *in vitro* experiments using two examples, both containing drugs routinely used in the clinic: (*i*) $[ZrO]^{2+}[BMP]^{2-}_{0.996}[DUT]^{2-}_{0.004}$, where the anti-inflammatory agent betamethasone phosphate was combined with the near-infrared emitting $[DUT]^{2-}$ dye for optical detection (Figures 3,4b), and (*ii*) $[ZrO]^{2+}[FdUMP]^{2-}$ containing the chemotherapeutic agent 5′-fluoro-2′-deoxyuridine 5′-monophosphate ($[FdUMP]^{2-}$) (Figure 4c), which is one of the active metabolites of 5-fluorouracil (5-FU), an antineoplastic drug widely used to treat cancer.

To test the anti-inflammatory potential of $[ZrO]^{2+}[BMP]^{2-}_{0.996}[DUT]^{2-}_{0.004}$, we first treated macrophages of the murine MHS cell line with endotoxine lipopolysaccharide (LPS, 200 ng mL^{-1}) to provoke an inflammatory response. Simultaneously, the macrophages were incubated for 48 h either with the anti-inflammatory drug dexamethasone (DM, 1×10^{-7} M) as a control or with $[ZrO]^{2+}[BMP]^{2-}_{0.996}[DUT]^{2-}_{0.004}$ IOH-NPs in concentrations ranging from 1×10^{-10} to 1×10^{-5} M (Figure 4b). The anti-inflammatory effects of the drugs were assessed by the use of an ELISA assay measuring the release of the cytokine tumor necrosis factor alpha (TNFα) into the culture medium. Increasing amounts of $[ZrO]^{2+}[BMP]^{2-}_{0.996}[DUT]^{2-}_{0.004}$ resulted in a dose-dependent reduction in TNFα secretion of LPS-stimulated macrophages, confirming that the inflammatory response was efficiently diminished by the IOH-NPs. Interestingly, the efficacy of 1×10^{-5} M $[ZrO]^{2+}[BMP]^{2-}_{0.996}[DUT]^{2-}_{0.004}$ compares to 1×10^{-7} M of dissolved molecular DM. Presumably, this can be attributed to a delayed release of the drug from the IOH-NPs by phosphatase-mediated hydrolysis.[22] While this effect may appear suboptimal at first sight, it could turn into an advantage under *in vivo* conditions where a constant, slow drug action is often desirable.[22] In view of a new class of nanomaterials with an exceptional load of active agent (81 wt % BMP in $[ZrO]^{2+}[BMP]^{2-}_{0.996}[DUT]^{2-}_{0.004}$), this result is very promising, all the more as targeted delivery and eventually reduced side effects have not been considered yet.

The antiproliferative potential of the second type, $[ZrO]^{2+}[FdUMP]^{2-}$ IOH-NPs with 75 wt % load of active FdUMP, is exemplarily shown on human MDA-MB-231 mammary carcinoma cells and compared to the nonactive $[ZrO]^{2+}[UMP]^{2-}$ (negative control) and to the clinically applied molecular drug 5-fluoruracil (5-FU, positive control) (Figure 4c). For $[ZrO]^{2+}[FdUMP]^{2-}$ at different points in time after administration (24 to 72 h) and concentrations of 0 to 250 μM, a strong time- and concentration-dependent decrease in cell viability was measured using a CellTiter 96 Kit. In contrast, the negative control $[ZrO]^{2+}[UMP]^{2-}$ IOH-NPs, containing the same amount of nonactive uridine monophosphate $[UMP]^{2-}$, had no effect on cell viability. Interestingly, the same amounts of molecular 5-FU (positive control) show lower antiproliferative effects and a higher cell viability as compared to the $[ZrO]^{2+}[FdUMP]^{2-}$ IOH-NPs (for example 40% viable cells upon 72 h of treatment with 25 μM IOH-NPs compared to 60% viable cells after 72 h of treatment with the same amount of 5-FU). From the one side, the results generally confirm the biocompatibility of $[ZrO]^{2+}[R_{function}OPO_3]^{2-}$ IOH-NPs, as no cytotoxic effects of the control probe $[ZrO]^{2+}[UMP]^{2-}$ were observed even upon 72 h of treatment with concentrations as high as 250 μM. From the other side, strong antiproliferative activity of the $[ZrO]^{2+}[FdUMP]^{2-}$ IOH-NPs is confirmed, which was even prominently higher than the effect of clinically applied 5-FU (Figure 4c). Although this effect requires much more detailed studies, a different behavior of the IOH-NPs and the dissolved molecular drug is obvious and might be related to the different membrane permeability and cell-uptake mechanisms of dissolved molecular drugs and solid nanoparticles.[25] Additional aspects such as side effects again require detailed follow-up studies to evaluate the full biomedical potential of the IOH-NPs.

In sum, both *in vitro* assays using either $[ZrO]^{2+}[BMP]^{2-}_{0.996}[DUT]^{2-}_{0.004}$ or $[ZrO]^{2+}[FdUMP]^{2-}$ indicate the

DOI: 10.1021/jacs.5b01172
J. Am. Chem. Soc. 2015, 137, 7329−7336

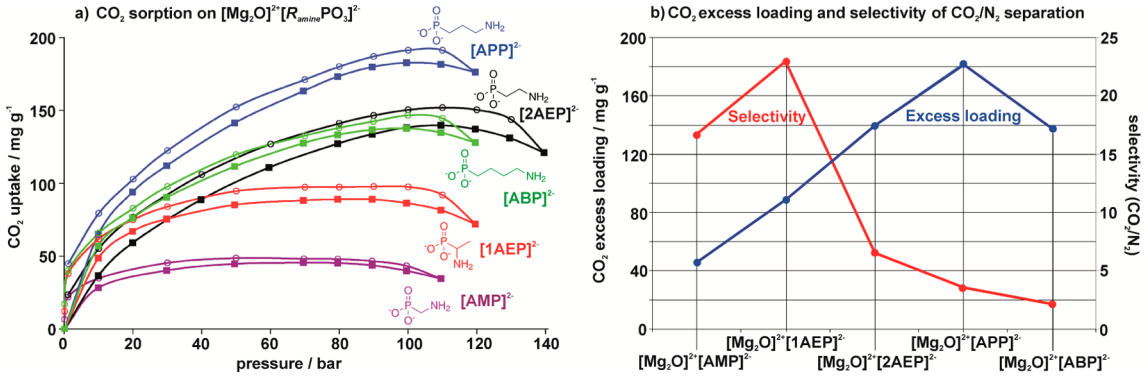

Figure 5. CO_2 sorption and separation based on $[Mg_2O]^{2+}[R_{amine}PO_3]^{2-}$ IOH-NPs: (a) CO_2 sorption of IOH-NPs with different functional anions $[R_{amine}PO_3]^{2-}$; (b) CO_2 excess loading and selectivity for CO_2/N_2 separation as calculated via IAST (SI: Table S3, Figures S13–S15). Gravimetric sorption analysis was performed at 80 °C for CO_2 and N_2.

successful drug release with anti-inflammatory or antiproliferatory activity, respectively. As exemplarily shown for $[ZrO]^{2+}$-$[BMP]^{2-}_{0.996}[DUT]^{2-}_{0.004}$, functional anions $[R_{drug}OPO_3]^{2-}$ and $[R_{dye}OPO_3]^{2-}$ can be combined, in principle, in variable ratios $[ZrO]^{2+}[R_{drug}OPO_3]^{2-}_{x}[R_{dye}OPO_3]^{2-}_{1-x}$. Thus, theranostic functionalities can be easily established with drug delivery and optical-detection properties merged in one nanoparticle (Figures 3, 4). Based on the straightforward aqueous synthesis and clinically approved materials such as $[BMP]^{2-}$ and $[FdUMP]^{2-}$, IOH-NPs can become acutely interesting for *in vitro* and *in vivo* medical application.

3.4. CO_2 Sorption and Separation via $[Mg_2O]^{2+}$-$[R_{amine}PO_3]^{2-}$ IOH-NPs. New concepts and materials for efficient CO_2 storage and separation are of general relevance in view of the global greenhouse effect. Based on existing materials for CO_2 sorption (e.g., hydrotalcites, lithium zirconate, calcium oxide, amine-modified porous oxides/zeolites, metalorganic frameworks/MOFs),[26] low-cost and easy-to-prepare sorption materials, preferentially with high selectivity, are still mandatory. Here, IOH-NPs with amine-containing functional anions $[R_{amine}PO_3]^{2-}$ can be an alternative. Hence, we have studied various aminoalkyl phosphonates $[R_{amine}PO_3]^{2-}$, including aminomethyl phosphonate (AMP), 1-aminoethyl phosphonate (1AEP), 2-aminoethyl phosphonate (2AEP), aminopropyl phosphonate (APP), and aminobutyl phosphonate (ABP) (Figures 1, 5). It must be noted that zirconium was replaced here by magnesium as the cation in the IOH-NPs in view of its lower weight.

The CO_2 uptake of all $[Mg_2O]^{2+}[R_{amine}PO_3]^{2-}$ IOH-NPs ranges between 40 and 180 mg g^{-1} up to a pressure of 120 bar (Figure 5a, Table 1). Reversible CO_2 sorption of the IOH-NPs proceeds via carbamate formation, analogous to liquid alkylamines or postsynthesis amine-functionalized MOFs: 2 RNH_2 + CO_2 ↔ $[RNH_3]^+$ + $[RNHCOO]^-$.[26a,27] The CO_2 uptake increases with the specific surface area and decreases with the molar weight of the IOH-NPs (Table 1). Furthermore, studies on amine-functionalized zeolites (e.g., SBA-12) have shown that the CO_2 uptake decreases with the alkyl-chain length of the alkylamine due to the reduced alkalinity of the amine group.[28] Based on these opposing effects, the highest CO_2 uptake is observed here for $[Mg_2O]^{2+}[2AEP]^{2-}$ and $[Mg_2O]^{2+}[APP]^{2-}$ (Figure 5a).

Table 1. Specific Surface Area, CO_2 and N_2 Uptake, and Selectivity of $[Mg_2O]^{2+}[R_{amine}PO_3]^{2-}$ IOH-NPs

compound	specific surface area (from BET analysis) $m^2\ g^{-1}$	CO_2 uptake mg g^{-1} (mmol g^{-1})	N_2 uptake mg g^{-1} (mmol g^{-1})	selectivity (IAST calculation) α (CO_2:N_2)
$[Mg_2O]^{2+}[AMP]^{2-}$	250	46 (1.0)	6 (0.2)	16.7
$[Mg_2O]^{2+}[1AEP]^{2-}$	258	89 (2.0)	14 (0.5)	23.0
$[Mg_2O]^{2+}[2AEP]^{2-}$	357	140 (3.2)	8 (0.3)	6.6
$[Mg_2O]^{2+}[APP]^{2-}$	532	182 (4.1)	25 (0.9)	3.6
$[Mg_2O]^{2+}[ABP]^{2-}$	436	138 (3.1)	14 (0.5)	2.2

In order to study the selectivity of CO_2 sorption, the N_2 uptake was determined as well for the $[Mg_2O]^{2+}[R_{amine}PO_3]^{2-}$ IOH-NPs at 80 °C up to 120 bar. For all compounds, the N_2 sorption is significantly lower as compared to CO_2 with 25 mg g^{-1} at maximum for $[Mg_2O]^{2+}[APP]^{2-}$ (Table 1; SI: Table S3, Figure S13). This confirms the interaction of acidic CO_2 with the base amino-function of the $[Mg_2O]^{2+}[R_{amine}PO_3]^{2-}$ IOH-NPs. A Langmuir isotherm model was used to fit the experimentally observed pure gas adsorption isotherms of CO_2 and N_2 and to calculate the selectivity via the ideal adsorbed solution theory (IAST; SI: Figures S14, S15). As a result, selectivities of α = 2.2–23.0 were obtained with $[Mg_2O]^{2+}[AMP]^{2-}$ (α = 16.7) and $[Mg_2O]^{2+}[1AEP]^{2-}$ (α = 23.0) having the highest values (Table 1, Figure 5b). Again, the specific surface area that increases for longer alkyl chains, and the alkalinity of the amine-function that is higher for short alkyl chains must be considered.[28] While the first effect favors high sorption capacities, the latter promotes high selectivity. In sum, the adsorption isotherms of $[Mg_2O]^{2+}[AMP]^{2-}$ and $[Mg_2O]^{2+}[1AEP]^{2-}$ show the steepest slopes at low pressure, and therefore a higher selectivity toward CO_2 as compared to the other IOH-NPs.

With this CO_2 uptake and selectivity, $[Mg_2O]^{2+}[AMP]^{2-}$ and $[Mg_2O]^{2+}[1AEP]^{2-}$ IOH-NPs can be promising new sorbents for CO_2 separation from N_2, all the more when considering their facile water-based synthesis. Although the maximum CO_2 uptake on MOFs is naturally much higher (up to 2,500 mg g^{-1}),[26a,29] the combination of uptake and selectivity of the IOH-NPs is meaningful. Taking both aspects together, the $[Mg_2O]^{2+}[R_{amine}PO_3]^{2-}$ IOH-NPs are very comparable to postsynthesis amine-modified MOFs with typical selectivities of α = 5–50 at capacities of 50 to 200 mg g^{-1} CO_2.[26a] In view of the temperature and pressure range being accessible with the IOH-NPs (up to 80 °C and 120 bar), especially, they can become relevant for high-pressure treatment (≥20 bar) (e.g., in precombustion/oxy-combustion processes, syngas sequestra-

DOI: 10.1021/jacs.5b01172
J. Am. Chem. Soc. 2015, 137, 7329–7336

tion, membrane separation processes).[26a,30] Here, the $[Mg_2O]^{2+}[R_{amine}PO_3]^{2-}$ IOH-NPs can be considered as a nanoscaled, solid-state alternative to the widely applied, but corrosive and volatile liquid alkylamines.[26]

4. CONCLUSIONS

In conclusion, we present phosphate-based inorganic−organic hybrid nanoparticles $[M]^{2+}[R_{function}(O)PO_3]^{2-}$ (IOH-NPs with M = ZrO, Mg_2O; R = functional organic group) as a new and general platform for addressing multipurpose properties. This includes full-color fluorescence based on $[ZrO]^{2+}[R_{dye}OPO_3]^{2-}$ IOH-NPs with the examples $[ZrO]^{2+}[PUP]^{2-}$ (blue emission), $[ZrO]^{2+}[MFP]^{2-}$ (green emission), $[ZrO]^{2+}[RRP]^{2-}$ (red emission), and $[ZrO]^{2+}[DUT]^{2-}$ (infrared emission). Drug transport and delivery is shown for $[ZrO]^{2+}[R_{drug}OPO_3]^{2-}$ IOH-NPs based on the anti-inflammatory and antitumor effect of $[ZrO]^{2+}[BMP]^{2-}$ and $[ZrO]^{2+}[FdUMP]^{2-}$. Both compounds exhibit exceptionally high loads of the active agent (81 wt % of BMP, 71 wt % of FdUMP). Moreover, theranostics can be realized by the merging of functional anions such as in the case of $[ZrO]^{2+}[BMP]^{2-}{}_{0.996}[DUT]^{2-}{}_{0.004}$ containing the anti-inflammatory agent betamethasone phosphate and the infrared-emitting dye Dyomics-647 uridine triphosphate. Finally, amine-based functional anions in $[MgO]^{2+}[R_{amine}PO_3]^{2-}$ IOH-NPs show CO_2 sorption (up to 180 mg g^{-1}) and can be used for CO_2/N_2 separation (selectivity up to α = 23). This includes aminomethyl phosphonate $[AMP]^{2-}$, 1-aminoethyl phosphonate $[1AEP]^{2-}$, 2-aminoethyl phosphonate $[2AEP]^{2-}$, aminopropyl phosphonate $[APP]^{2-}$, and aminobutyl phosphonate $[ABP]^{2-}$.

Besides the synthesis of phosphate-based inorganic−organic hybrid nanoparticles as a new class of nanoparticles, the wide adaptability of material composition and properties and the noncomplex water-based synthesis are major advantages for practical handling and a difference from many yet established synthesis and material concepts. Especially, for biomolecular and medical application, the use of less-harmful, partly clinically approved constituents such as $[BMP]^{2-}$ and $[FdUMP]^{2-}$ can be highly relevant for biomedical application. The flexible combination of functional anions leading to a general composition $[ZrO]^{2+}([R_{drug}OPO_3]_{1-x}[R_{dye}OPO_3]_x)^{2-}$ leads to promising potential in theranostics. Based on the concept of IOH-NPs, in principle, the merging of other phosphate-based functional anions can lead to many more nanoparticles with adaptable composition and flexible properties.

■ ASSOCIATED CONTENT

Supporting Information

Details of analytical tools, synthesis of the phosphate-based IOH-NPs, materials characterization of the as-prepared IOH-NPs, cell-based analysis and *in vivo* imaging, gas sorption and separation. The Supporting Information is available free of charge on the ACS Publications website at DOI: 10.1021/jacs.5b01172.

■ AUTHOR INFORMATION

Corresponding Authors

*falves@gwdg.de

*claus.feldmann@kit.edu

Author Contributions

J.G.H. and J.N equally contributed to the manuscript and data acquisition. J.G.H. and S.S. designed and performed synthesis, chemical characterization and gas sorption experiments, collected and analyzed the data. J.N. designed, performed and analyzed all the in vitro cell culture experiments and in vivo imaging. C.F. and F.A. developed the materials concept, supervised the project, discussed strategy and results, and wrote the manuscript which was edited and approved by all co-authors. H.M.R. contributed to the cell culture experiments. M.L., J.M. and R.S. approved all sorption data.

Notes

The authors declare no competing financial interest.

■ ACKNOWLEDGMENTS

J.G.H., S.S., and C.F. are grateful to the Deutsche Forschungsgemeinschaft (DFG) for funding of the experimental equipment. J.G.H. and C.F. thank Nicole Klaassen for excellent technical assistance. Moreover, J.N., F.A., and H.M.R. express their gratitude to Bärbel Heidrich and Amina Bassibas for excellent technical assistance.

■ REFERENCES

(1) Shi, J. *Chem. Rev.* **2013**, *113*, 2139−2181.

(2) Cheng, Z.; Al Zaki, A.; Hui, J. Z.; Muzykantov, V. R.; Tsourkas, A. *Science* **2012**, *338*, 903−910.

(3) Schmidt, M. A.; Lei, D. Y.; Wondraczek, L.; Nazabal, V.; Maier, S. A. *Nat. Commun.* **2012**, *3*, 2109/1−2109/8.

(4) Chung, I.; Lee, B.; He, J.; Chang, R. P. H.; Kanatzidis, M. G. *Nature* **2012**, *485*, 486−489.

(5) Park, Y.; Petit, C.; Han, P.; Park, A. *RSC Adv.* **2014**, *4*, 8723−8726.

(6) Chung, J. J.; Castro, C. M.; Im, H.; Lee, H.; Weissleder, R. *Nat. Nanotechnol.* **2013**, *8*, 369−375.

(7) Benson, O. *Nature* **2011**, *480*, 193−199.

(8) Park, D. H.; Kim, M. S.; Joo, J. *Chem. Soc. Rev.* **2010**, *39*, 2439−2452.

(9) (a) Xu, P.; Han, X.; Zhang, B.; Du, Y.; Wang, H. L. *Chem. Soc. Rev.* **2014**, *43*, 1349−1360. (b) Kao, J.; Thorkelsson, K.; Bai, P.; Rancatore, B. J.; Xu, T. *Chem. Soc. Rev.* **2013**, *42*, 2654−2678.

(10) (a) Shearer, C. J.; Cherevan, A.; Eder, D. *Adv. Mater.* **2014**, *26*, 2295−2318. (b) Soler-Illia, G. J. A. A.; Azzaroni, O. *Chem. Soc. Rev.* **2011**, *40*, 1107−1150.

(11) (a) Wei, G.; Ma, P. X. *Adv. Funct. Mater.* **2008**, *18*, 3568−3582. (b) Aili, D.; Stevens, M. *Chem. Soc. Rev.* **2010**, *39*, 3358−3370.

(12) Sanchez, C.; Lebeau, B.; Chaput, F.; Boilot, J.-P. *Adv. Mater.* **2003**, *15*, 1969−1994.

(13) (a) Sailor, M. J.; Park, J.-H. *Adv. Mater.* **2012**, *24*, 3779−3802. (b) Park, Y.-S.; Advincula, R. C. *Chem. Mater.* **2011**, *23*, 4273−4294. (c) Cortie, M. B.; McDonagh, A. M. *Chem. Rev.* **2011**, *111*, 3713−3735. (d) Costi, R.; Saunders, A. E.; Banin, U. *Angew. Chem., Int. Ed.* **2010**, *49*, 4878−4897.

(14) (a) Roming, M.; Feldmann, C. U.S. Patent, US 12/867,348. (b) Roming, M.; Lünsdorf, H.; Dittmar, K. E. J.; Feldmann, C. *Angew. Chem., Int. Ed.* **2010**, *49*, 632−637. (c) Heck, J.; Poß, M.; Napp, J.; Alves, F.; Stühmer, W.; Feldmann, C. *Patent application*, DE 102014004512.9.

(15) La Mer, V. K.; Dinegar, R. H. *J. Am. Chem. Soc.* **1950**, *72*, 4847−54.

(16) Fujimoto, J. G.; Farkas, D. *Biomedical Optical Imaging*; Oxford University Press: Oxford, 2009.

(17) (a) Chen, O.; Zhao, J.; Chauhan, V. P.; Cui, J.; Wong, C.; Harris, D. K.; Wei, H.; Han, H.; Fukumura, D.; Jain, R. K.; Bawendi, M. G. *Nat. Mater.* **2013**, *12*, 445−451. (b) Zhu, Z.-J.; Yeh, Y.-C.; Tang, R.; Yan, B.; Tamayo, J.; Vachetand, R. W.; Rotello, V. M. *Nat. Chem.* **2011**, *3*, 963−968.

(18) (a) Liu, Y.; Tu, D.; Zhu, H.; Chen, X. *Chem. Soc. Rev.* **2013**, *42*, 6924−6958. (b) Binnemans, K. *Chem. Rev.* **2009**, *109*, 4283−4374.

(19) Vivero-Escoto, J. L.; Huxford-Phillips, R. C.; Lin, W. *Chem. Soc. Rev.* **2012**, *41*, 2673−2685.

DOI: 10.1021/jacs.5b01172
J. Am. Chem. Soc. 2015, 137, 7329−7336

(20) Weissleder, R. *Nat. Biotechnol.* **2001**, *19*, 316−317.
(21) Mbawuike, I. N.; Herscowitz, H. B. *J. Leukoc. Biol.* **1989**, *46*, 119−127.
(22) Pradere, U.; Garnier-Amblard, E. C.; Coats, S. J.; Amblard, F.; Schinazi, R. F. *Chem. Rev.* **2014**, *114*, 9154−9218.
(23) (a) Wallace Hayes, A. *Principles and methods of toxicology*, 5th ed.; Taylor & Francis: New York, 2008; pp 876−878. (b) Greim, H. *The MAK collection for occupational health and safety*, Vol. *12*; Wiley-VCH: Weinheim, 2006; pp 223−236.
(24) Davis, M. E. *MRS Bull.* **2012**, *37*, 828−835.
(25) Balmert, S. C.; Little, S. R. *Adv. Mater.* **2012**, *24*, 3757−3778.
(26) (a) Sumida, K.; Rogow, D. L.; Mason, J. A.; McDonald, T. M.; Bloch, E. D.; Herm, Z. R.; Bae, T.-H.; Long, J. R. *Chem. Rev.* **2012**, *112*, 724−781. (b) Nugent, P.; Belmabkhout, Y.; Burd, S. D.; Cairns, A. J.; Luebke, R.; Forrest, K.; Pham, T.; Ma, S.; Space, B.; Wojtas, L.; Eddaoudi, M.; Zaworotko, M. J. *Nature* **2013**, *495*, 80−84.
(27) Leidinger, P.; Simonato, S.; Feldmann, C. *Chem. Commun.* **2012**, *48*, 7046−7048.
(28) Zelenak, V.; Halamova, D.; Gaberova, L.; Bloch, E.; Llewellyn, P. *Microporous Mesoporous Mater.* **2008**, *116*, 358−364.
(29) Furukawa, H.; Ko, N.; Go, Y. B.; Aratani, N.; Choi, S. B.; Choi, E.; Yazaydin, A. Ö.; Snurr, R. Q.; O'Keeffe, M.; Kim, J.; Yaghi, O. M. *Science* **2010**, *329*, 424−428.
(30) Li, F.; Fan, L. S. *Energy Environ. Sci.* **2008**, *1*, 248−267.

DOI: 10.1021/jacs.5b01172
J. Am. Chem. Soc. 2015, 137, 7329−7336